Energy Consumption Models for Delivery Drones: A Comparison and Assessment

Preprint · May 2020

4 authors:

Juan Zhang
University of Wisconsin - Eau Claire
7 PUBLICATIONS **68** CITATIONS
SEE PROFILE

James F. Campbell
University of Missouri - St. Louis
99 PUBLICATIONS **5,005** CITATIONS
SEE PROFILE

Donald C Sweeney
University of Missouri - St. Louis
19 PUBLICATIONS **285** CITATIONS
SEE PROFILE

Andrea C. Hupman
University of Missouri - St. Louis
14 PUBLICATIONS **74** CITATIONS
SEE PROFILE

Energy Consumption Models for Delivery Drones: A Comparison and Assessment

May 30, 2020

Juan Zhang[1], James F. Campbell[2], Donald C. Sweeney II[3], Andrea C. Hupman[4]
College of Business Administration, University of Missouri-St. Louis, USA 63121
[1]jzmq3@mail.umsl.edu, [2]campbell@umsl.edu, [3]sweeneyd@umsl.edu, [4]hupmana@umsl.edu

Abstract

Energy consumption is a critical constraint for drone delivery operations to achieve their full potential of providing fast delivery, reducing cost, and cutting emissions. This paper provides a uniform framework to facilitate understanding different drone energy consumption models and the inter-relationships between key factors and performance measures to facilitate decision making for drone delivery operations. We review, classify and assess drone energy consumption models. We then document the very wide variations in the modeled energy consumption rates resulting from differences in: (1) the scopes and features of the models; (2) the specific designs of the drones; and (3) the details of their assumed operations and uses. The results show that great care must be taken in adopting a particular drone energy consumption model and that more research is needed, especially empirical research, to ensure the selected model accurately reflects delivery drone designs and uses.

Keywords: unmanned aerial vehicle, UAV, drone, drone energy models, energy consumption, parcel delivery

1. Introduction

Unmanned Aerial Vehicles (UAVs) or drones have been proposed as a method for delivering goods to consumers with benefits of lower cost, increased speed, and reduced greenhouse gas emissions. For drone delivery, the drone energy requirements determine the key

performance metrics of range (or endurance), cost and emissions. However, many optimization models that design drone or truck-drone routes or drone delivery systems incorporate energy consumption only indirectly as a fixed limit on drone endurance (flight time limit) or range (flight distance limit) (e.g., Murray and Chu, 2015; Chiang et al., 2019; Kitjacharoenchai et al 2020). Other drone delivery research incorporates energy directly with an energy consumption model based on the fundamental physical forces involved in flight or on field measurements (e.g., Kirschstein 2020; Murray and Raj 2020; Poikonen and Golden, 2020; Stolaroff et al., 2018; Figliozzi, 2017; Dorling et al., 2017). Some of these drone energy consumption models are quite simple, such as the integrated lift-drag model or regression models, while others are comprised of multiple components to include detailed representations of the forces of flight and drone design.

However, these various drone energy models can produce widely divergent results in terms of the energy consumed, which leads to wide differences in modeled drone ranges and emissions for essentially the same drone delivery operations. This creates the need to carefully delineate why such differences exist when modeling the same phenomena (i.e. drone flights or drone delivery) and to assess the different approaches to modeling drone energy consumption. We limit our consideration to battery-powered aerial drones, such as proposed for home delivery operations (Lee, 2019; Josephs, 2019) and related activities (e.g., medical deliveries over short ranges (Cohen, 2019; Drones in HealthCare, 2020)).

The wide variation of energy consumption in published drone delivery research results from different scopes and features in the models, different designs of the drones being modeled, and different assumed operations. Thus, current research has not reached consensus on how to model delivery drone energy consumption – and existing models may not reflect drone delivery operations well. The key contributions of this paper are to: (1) review and classify key published

drone energy consumption models using a unified notation that allows a collective comparison of the energy consumption rates for the various drone types, payloads, speeds, etc.; (2) examine how the distinguishing features of different drone energy consumption models contribute to differences in the calculated energy consumption; (3) evaluate published results on energy consumption for small, medium and heavy delivery drones from both the models and field tests; and (4) compare the drone energy consumption models in a common setting to document how energy use and range vary differentially as a function of speed and payload. We believe the results provide useful insights for modeling energy consumption for current drones, as well as for future (not yet existing) drones.

The rest of the paper is organized as follows. Section 2 provides background and classification of drone energy consumption models in the literature. Section 3 discusses key drone energy consumption models using a unified notation. Section 4 documents the differences in the energy consumption rates as reported in the literature as well as in a common setting. Section 5 discusses insights and implications of the analyses, and Section 6 provides concluding remarks.

2. Background and features of drone energy consumption models

2.1 Background

Key factors affecting drone energy consumption can be classified into four categories: drone design, environment, drone dynamics, and delivery operations. Major factors in these four categories are provided in Figure 1 (adapted from Demir et al. (2014) for road transport). Drone design factors include the weight and size of the drone body, the number and size of rotors, the weight, size and energy capacity of the battery, power transfer efficiency, maximum speed and payload, lift-to-drag ratio, delivery mechanism and avionics. Environmental factors include air density, gravitational force, wind conditions, weather (snow, rain, etc.), ambient temperature and

operating regulations. Drone dynamics factors include drone travel speed, drone motion (i.e., takeoff/landing, hover, horizontal flight), acceleration/deceleration, angle of attack and flight altitude. Delivery operations factors include weight and size of the payload, "empty returns" (i.e. the return trip after delivery is without the payload, which implies a successful delivery), fleet size and mix, the number of deliveries per trip and the area of the service region. Some of these factors are determined or limited by the drone design (e.g., maximum payload, projected area of the drone, etc.), others are operational factors that can vary for a given drone design (e.g., payload, speed, etc.), and still others are external factors (e.g., weather). Further, many of these factors are interdependent and also dynamic during a drone delivery trip.

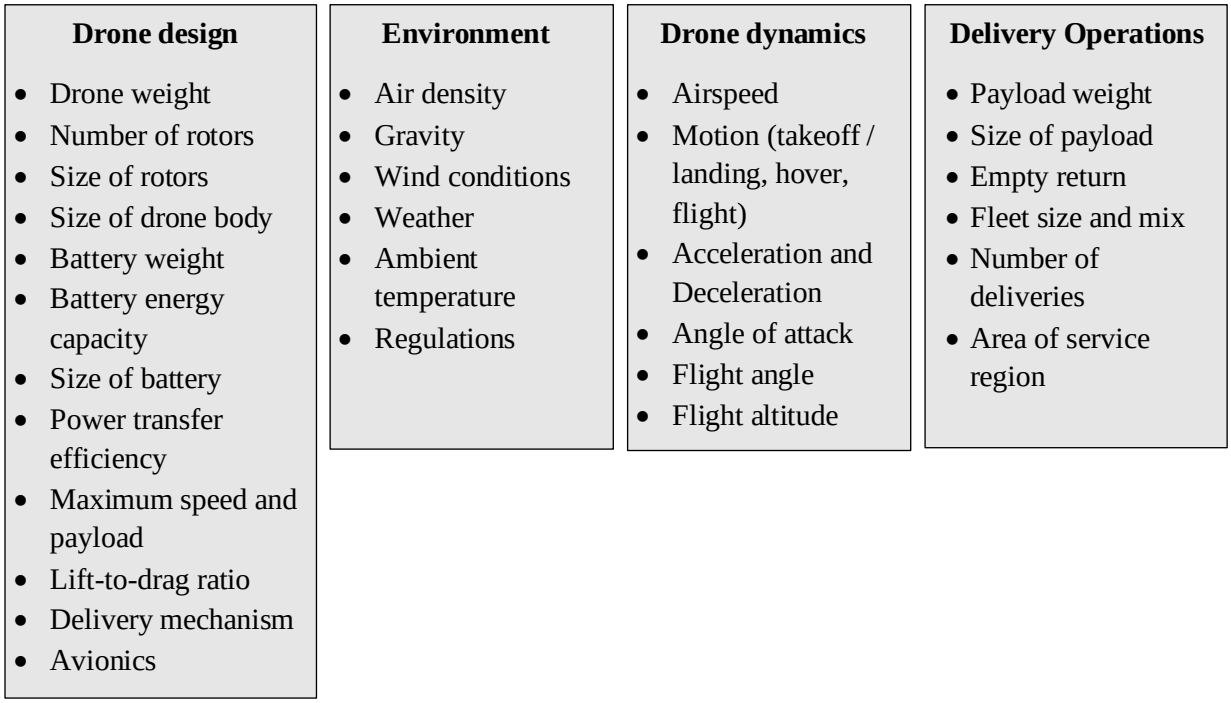

Figure 1. Factors affecting drone energy

A drone uses energy to fly by generating thrust and lift forces to overcome the weight and drag forces. Figure 2 highlights five key interrelated aspects of drone energy consumption: payload weight, battery weight, drone (airframe) weight, airspeed, and range. The airspeed, payload, drone

weight and battery weight are important determinants of the drone energy consumption rate. The energy consumption rate in turn, along with the battery weight (and type), determines the range. Note that the payload, drone and battery weight determine the total weight of the drone at takeoff, and involve both design decisions (drone and battery weight) and operating decisions (payload weight). Increasing the weight of any component increases the energy consumption rate, ceteris paribus, as indicated by the "(+)" on the three arrows from the weights to the energy consumption rate. Airspeed is an operating decision, and for drones (as well as airplanes and helicopters) the power consumed is approximately a convex function of airspeed (due to the competing forces of induced drag, parasite drag, and profile drag – see for example Rotaru and Todorov (2017)). Thus, there is a "(+/-)" on the arrow out of Airspeed. Range is determined by both the drone design and operating decisions. Note that an increase in battery weight will increase the drone energy consumption rate, ceteris paribus, which decreases the range; but the larger battery will also increase the available energy capacity, which increases the range (see Stolaroff et al. (2018) for a discussion of how battery size affects drone energy use and range).

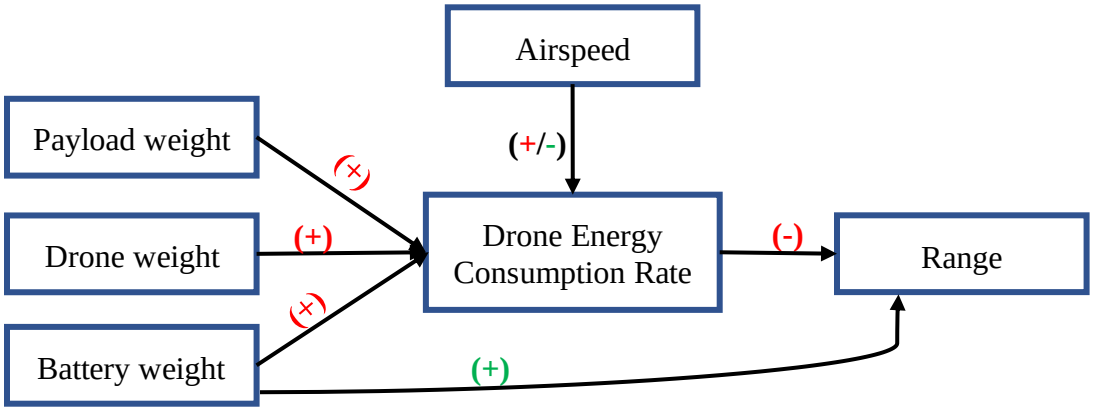

Figure 2. Interrelated aspects of the energy consumption rate for drone delivery

2.2 Relevant literature and key drone energy models

Since the seminal work of Murray and Chu (2015), many researchers have considered designing and optimizing drone delivery, either from a depot and/or with truck-drone combinations. This includes drone routing and scheduling (e.g., Dorling et al., 2017; Agatz et al., 2018; Schermer et al., 2019; Liu, 2019; Murray and Raj, 2020; Kitjacharoenchai et al., 2020), location problems including for charging stations (Chauhan et al., 2019; Shavarani et al., 2018; Hong et al., 2018; Ferrandez et al., 2016), and fleet sizing (Troudi et al., 2018). See Otto et al. (2018) for a survey of drone modeling.

Some optimization models have incorporated drone energy consumption models explicitly, with a key differentiation being the assumption regarding thrust for steady horizontal flight. The model may assume that (i) the thrust force (T) equals the drag force (D), and the weight force (W) equals the lift force (L) (therefore, $T = W/r$, where $r = L/D$ is the lift-to-drag ratio), (ii) the thrust force equals the weight force, as for a hovering helicopter, or (iii) the thrust force equals the sum of the weight, the drag and the lift forces. These different assumptions reflect different perspectives on the drone operations, e.g., whether they operate more like fixed-wing aircraft or helicopters. These three approaches give rise to three continuing streams of literature for drone energy modeling. Key references are described briefly in this section, with details in Section 3.

D'Andrea (2014) provides a seminal contribution in modeling drone energy consumption by translating the fundamental flight principles of manned aircraft to a model for the much smaller scale of unmanned aerial drones. This article presents a model using an integrated approach that combines aerodynamic and drone design aspects into a single critical parameter: the lift-to-drag ratio r. The energy model also includes a fixed component for avionics power. Troudi et al. (2018) uses the same model to analyze drone fleet size, though they ignore the avionics power. Figliozzi

(2017) adopts the same modeling approach and uses it to derive drone emissions based on a continuous approximation travel distance model. The D'Andrea integrated model is also used in a series of reports from the RAND Corporation that explore energy consumption for city-scale drone delivery systems (Lohn, 2017; Xu, 2017; Gulden, 2017). Lohn (2017) uses this model to analyze truck and drone delivery in cities of various sizes, and Gulden (2017) provides a GIS-based analysis of shifting truck deliveries to drones in Minneapolis. Xu (2017) discusses vehicle design aspects related to drone energy consumption and suggests that fixed-wing VTOL (vertical takeoff and landing) or hybrid multicopter configurations that combine VTOL capabilities with lifting surfaces (wing-like structures) are a better fit for many drone delivery operations. Several such drones have been tested, including the latest delivery drone designs of Amazon, Google, and others (Lee, 2019; Heath, 2018; Adams, 2016; Swoop Aero, 2019).

A different approach for modeling drone energy consumption is based on helicopter operations, with the assumption that the power consumed during level flight, takeoff, or landing is approximately equivalent to the power consumed while hovering. Dorling et al. (2017) provides an equation for the power consumed by a multirotor helicopter in hover as a function of the battery and payload weight. These authors also report field experiments and develop regression parameters with small payloads (see Section 3.3). Jeong et al. (2019) adapts Dorling's hovering model for a MikroKopter MK8-3500 drone, and also describe a regression model based on payload mass. They state the "proposed energy consumption model provides realistic values that are analogous to the experiment result"; however, they do not provide any parameter values for the model.

The third approach is comprised of component models based on the fundamental forces of flight, including the weight force of the aircraft (due to gravity) and drag forces. The two main drag forces acting on aircraft are parasite drag from the aircraft moving through the atmosphere

and induced drag from redirecting the airflow to create the lift that keeps the aircraft aloft. Component models for drone energy consumption include separate models for the individual forces and the different components of a drone trip (takeoff, landing, cruising, hovering), and are often quite detailed to capture particular features of the drone design. Stolaroff et al. (2018) develops a two-component model based on the thrust required to balance the drone weight and the parasite drag force. This is used to assess the energy use and life cycle greenhouse gas (GHG) emissions for small drones with short ranges (4 km) delivering from warehouses. Results indicate that small drones are likely to provide lower lifecycle GHG emissions than conventional delivery trucks, but that benefits depend on the carbon intensity of electricity and the size of drones. Liu et al. (2017) provide a detailed three component drone energy model that includes power to maintain lift and overcome parasite drag (as in Stolaraoff et al. 2018), along with profile power to overcome the rotational drag of the propeller blades. Field tests in Liu et al. (2017) show that ascending takes 9.8% more power than hovering, and descending takes 8.5% less power than hovering (similar to results in Di Franco and Buttazzo (2015)). Kirschstein (2020) uses a similar component model, but in an idealized delivery process from a depot with separate energy calculations for takeoff and ascent, steady level flight, descent, hovering, and landing for delivery. The return trip is similar but without the payload. Kirschstein (2020) compares delivery with trucks versus drones for Berlin and shows that drone delivery often requires more energy. The results also highlight how wind and drone hovering increase energy consumption. Several other authors have developed component drone power and energy models similar to those above for problems involving drones in wireless communication networks (e.g., Zeng and Zhang, 2017; Zeng, 2019; Wu, 2019).

A final approach to modeling drone energy consumption is with regression based on field experiments, as in some articles previously mentioned. Tseng et al. (2017a, 2017b) present a nine-

term nonlinear regression model for drone power consumption that includes horizontal and vertical speed and acceleration, as well as payload mass and wind speed.

Murray and Raj (2020) design truck-drone tandem delivery routes with a three-phase heuristic and is the only reference to consider multiple drone energy models, including the model of Liu et al. (2017), a simple regression model that is linear in payload, and models with a fixed distance or time limit (essentially modeling energy consumption as a linear function of drone travel distance or time). Relevant findings for our study were that (i) the different energy models can produce very different routes, with several energy models leading to the creation of energy infeasible drone routes, and (ii) it is important to include the energy consumed outside the steady level flight portion of a delivery trip (e.g., for launch, retrieval and delivery), especially for any hovering needed for coordination with a truck or other drones prior to landing.

Table 1 provides a categorization of 12 key drone energy consumption models in common terms. Column 1 identifies the reference for the model. Columns 2-4 identify the assumption regarding thrust for steady horizontal flight and show the three groupings of models as discussed earlier. Columns 5-7 reflect the scope of drone travel included in the model for the different drone flight segments (horizontal flight, hover, and vertical flight including takeoff/landing). Note that all 12 models for drone delivery include energy use for horizontal travel, but only half include energy for hovering and vertical travel. Columns 8-10 indicate adjustments to the modeled energy consumption for wind, avionics, and empty returns. Note that only 2 models do not include at least one of the three adjustments in columns 8-10, although these adjustments are often removed from the models in the reported computational results. Columns 11-12 indicate the type of model provided (either theoretical based on modeling thrust as in columns 2-4, or regression models) and show that 10 articles provide theoretical models, while 3 papers present regression models.

Column 13 indicates the five references that include field tests with a drone, often used for setting parameter values in the model.

3. Theoretical models for energy consumption

In this section, we discuss the theoretical models for energy consumption of each of the 12 articles in Table 1. We first provide in sub-section 3.1 a unified notation to facilitate comparison of all models. We then discuss in sub-section 3.2 the models that use an integrated approach (with the lift-to-drag ratio), followed in sub-section 3.3 by the models that use a component approach. For consistency we report all energy values in Joules (1 Joule = 1 Watt-second) and energy consumption rate for steady level flight (Epm) in Joules/meter.

3.1 Unified notation

Different authors use different notation for the same concepts, so to facilitate the understanding and comparison of the models, we employ the unified notation in Table 2 (m = meter; s = seconds; J = joules). We classify the drone physical components into three categories: (i) drone body (including the airframe, propellers, motors, sensors, GPS, avionics, and a camera if used), (ii) drone battery, and (iii) payload (package). Thus, the drone body includes everything except the battery and package. Two areas that sometimes cause confusion in the literature concern the range and the battery usage. We use R to denote the maximum distance that a drone can travel in one direction and still be able to return to the depot, i.e., half of the round-trip distance for an out-and-back delivery. We define η as the power transfer efficiency, which is the energy loss from battery to the propeller. Figliozzi (2017) uses an overall power transfer efficiency, which also includes the energy loss from charging to battery, to denote power transfer efficiency. This definition will result in a value a little smaller than η, as charging is not 100% efficient.

Table 1. Summary of key features of the models of drone energy consumption

Reference	Thrust Assumption for Flight			Travel Components			Wind	Avionics	Empty return	Theoretical Model	Regression Model	Field Tests
	i T=W/r	ii T=W	iii T=W+D+L	Horizontal	Hover	Vertical						
D'Andrea (2014)	x			x			x	x		x		
Figliozzi (2017)	x			x					x	x		
Dorling et al. (2017)		x		x	x	x				x	x	x
Tseng et al. (2017a)				x	x	x	x	x			x	x
Tseng et al. (2017b)				x	x	x	x	x			x	x
Liu et al. (2017)			x	x	x	x	x			x		x
Lohn (2017)	x			x	x	x	x	x	x	x		
Xu (2017)	x			x	x	x	x	x	x	x		
Stolaroff et al. (2018)			x	x			x		x	x		x
Troudi et al. (2018)	x			x				x		x		
Jeong et al. (2019)		x		x						x	x	
Kirschstein (2020)			x	x	x	x	x	x	x	x		

Notes for energy consumption adjustments: Including avionics increases energy consumption, while modeling empty returns decreases energy consumption (the return trip has lower weight). Wind is often modeled as increasing drone energy consumption (e.g., D'Andrea (2014)), though more detailed analyses show the energy use may increase or decrease depending on wind speed and direction and drone type (e.g., headwinds may increase lift, thereby reducing the power requirements; see Kirchstein (2020) for a detailed analysis of wind effects).

Table 2. Unified notation for drone energy models

$\rho =$ air density [kg/m^3] (e.g., 1.225 kg/m^3 at 15° C at sea level)
$g =$ acceleration of gravity [m/s^2]
$v_i =$ induced speed [m/s] (the change in the speed of the air after it flows through an object)
$v_a =$ airspeed [m/s] (speed of drone relative to the air)
$\varphi =$ ratio of headwind to airspeed [unitless]
$v =$ drone ground speed [m/s], so $v = (1 - \varphi)v_a$
$d =$ drone one-way travel distance for a single delivery trip [m]
$r =$ lift-to-drag ratio [unitless]
$\eta =$ battery and motor power transfer efficiency (from battery to propeller) [unitless]
$\eta_c =$ battery charging efficiency [unitless]
$k =$ index of the drone components: drone body=1; drone battery=2; payload (package)=3
$C_{D_k} =$ drag coefficient of drone component k [unitless]
$A_k =$ projected area of drone component k [m^2]
$m_k =$ mass of drone component k [kg]
$\gamma =$ maximum depth of discharge of the battery [unitless]
$s_{batt} =$ specific energy of the battery (energy capacity per kg) [J/kg]
$f =$ safety factor to reserve energy in the battery for unusual conditions [unitless]
$R =$ maximum one-way distance of drone travel per battery charge [m]
$P =$ power required to maintain a steady drone flight [Watt=J/s]
$P_{avio} =$ power required for all avionics on the drone (independent of drone motion) [Watt=J/s]
$n =$ number of rotors for a rotocopter drone [rotors]
$N =$ number of blades in one rotor for a rotocopter drone [blades]
$c =$ blade chord length [m]
$c_d =$ blade drag coefficient [unitless]
$\varsigma =$ area of the spinning blade disc of one rotor [m^2]
$\alpha =$ drone angle of attack [radians]
$Epm =$ energy required for steady drone flight per unit distance [J/m]

3.2 Energy models using integrated approaches

The seminal integrated model is provided by D'Andrea (2014) and is based on the ratio of lift-to-drag, r. This is a simple formula for calculating the power consumption (in kJ/s) required for the drone to maintain steady flight and operate on-board electronics in terms of the drone total mass, its speed, the lift-to-drag ratio, and the battery's power transfer efficiency. The derivation of this model is given in Appendix A. With no wind, D'Andrea (2014) provides the expression

$$P = \frac{\sum_{k=1}^{3} m_k v}{370 r \eta} + P_{avio}\ , \tag{1}$$

where the constant 370 (370 = 3600/9.8) allows velocities to be expressed in km/h rather than meters per second. In this paper, we express all speeds in m/s, so the equivalent expression is

$$P = \frac{(\sum_{k=1}^{3} m_k) g v_a}{r \eta} + P_{avio}. \tag{2}$$

The energy consumed for steady flight over a distance d is the power multiplied by the travel time d/v, so the energy per meter of travel (Epm) is the power divided by the speed

$$Epm = \frac{P}{v_a}\ , \tag{3}$$

So, for D'Andrea (2014) including possible headwinds as indicated via the unitless factor $\varphi = \frac{headwind\ speed}{drone\ airspeed}$, we have

$$Epm = \frac{1}{1-\varphi}\left(\frac{g \sum_{k=1}^{3} m_k}{r \eta} + \frac{P_{avio}}{v_a}\right). \tag{4}$$

One example in D'Andrea (2014) with no headwind ($\varphi = 0$), uses $m_1 = m_2 = m_3 = 2$ kg, $v_a = 12.5$ m/s (45 km/hr), $r = 3, \eta = 0.5$ and $P_{avio} = 100$ J/s. This requires total power of $P = 590$ J/s, or $Epm = 46.9$ J/m. With an 8.33 m/s headwind (30 km/hr) and other values as above, the energy consumption triples to $Epm = 140.8$ J/m. In D'Andrea (2014), the avionics consume about 17% of the total power for steady flight. Without avionics, $Epm = 38.9$ J/m when

there is no headwind, and $Epm = 116.8$ J/m with an 8.33 m/s headwind. Troudi (2018) uses the same model as described in eq.(2) with a MD4-1000 drone with a battery of 1,040,400 Joules (or 289Wh), $m_3 = 1.2$ kg, $m_1 + m_2 + m_3 = 5.55$ kg, and $v_a = 13$ m/s.

Figliozzi (2017) extends the basic model from D'Andrea (2014) for "steady flight" to consider empty returns. This model does not include power for avionics ($P_{avio} = 0$), models the lift-to-drag ratio as dependent on speed (with $r(v)$), and provides a unitless parameter for battery recharging efficiency (η_r). The overall energy consumption rate per unit distance (with no headwind) is given as

$$Epm = \frac{1}{2}\left(\frac{g\sum_{k=1}^{3} m_k}{r(v)\eta\eta_r} + \frac{g\sum_{k=1}^{2} m_k}{r(v)\eta\eta_r}\right). \quad (5)$$

The first term in parentheses is the energy consumption rate with a package, and the second term is the energy consumption rate without a package on the return trip.

The parameters used by Figliozzi (2017) are for a MicroDrones MD4-3000 and are as follows: $m_1 + m_2 = 10.1$ kg, $m_3 = 5$ kg, and the drone has a range of 36 km, though the paper suggests 70% of this, or 25 km, as the maximum range to provide a safety margin and allow for "unknown factors that can increase energy consumption such as headwinds". The lift-to-drag ratio $r(v)$ is not specified; however the article reports an Epm value of 77.8 J/m "calculated utilizing manufacturer information" and an overall power efficiency product of $\eta\eta_r = 0.9 * 0.73 = 0.66$. From these values, the lift-to-drag ratio can be calculated in reverse as $r = 2.4$. The article also assumes Epm values for a future more efficient drone at 38.9 J/m (half of the baseline value) and for a drone in "adverse conditions" (e.g., high winds) at 116.7 J/m (50% above the baseline value). This article uses a battery of 2.8 million Joules (or 777Wh).

The energy model used in the RAND Corporation studies (Lohn, 2017; Xu, 2017; Gulden, 2017) is based on D'Andrea (2014) and described in Lohn (2017). Lohn (2017) reports that for

truck and drone delivery serving a city the size of Los Angeles (1500 km^2) from a centrally located drone depot, the average energy use rate is Epm =112.5 J/m (assuming uniformly distributed deliveries in a circular city). Xu (2017) models a complete drone delivery mission that includes ascending to 150 m of altitude, flying level at 22.2 m/s (80 km/hr) into a 2.8 m/s (10 km/hr) headwind and then descending to the delivery site, with 30 seconds of hovering. The return trip is similar but without the payload and also includes flying into a 2.8 m/s headwind. Results are provided for a baseline multicopter design based on an Amazon Prime Air VTOL drone with 8 lift rotors and 2 cruise motors and the lift-to-drag ratio $r = 3$. For this baseline hybrid drone (weighing 55 lbs with a 20 mile range), Xu (2017) provides an energy consumption of 5.4 MJ for a 2.3 kg payload flying 32.2 km, resulting in $Epm = 168$ J/m. Xu (2017) indicates for a small drone with an 8 km delivery range, the energy consumption would be 1.44 MJ for the same payload flying 16 km, resulting in $Epm = 90$ J/m. He also considers an "advanced design" drone with future improvements in drone and battery design to achieve $r = 5.6$, for which flying a 2.3-kg payload 32.2 km roundtrip provides $Epm = 29$ J/m.

3.3 Component approaches

Dorling et al. (2017) provides a model for drone energy consumption based on hovering only (with the assumption that this is approximately equal to the energy for drone travel). During hover, the airspeed is zero, and the thrust balances the weight force, so

$$T = g \sum_{k=1}^{3} m_k \ . \tag{6}$$

Based on helicopter theory (e.g., Leishman (2002)), the power required for the drone to hover is

$$P = \frac{T^{3/2}}{\sqrt{2n\rho\varsigma}} = \frac{\left(g \sum_{k=1}^{3} m_k\right)^{3/2}}{\sqrt{2n\rho\varsigma}}, \tag{7}$$

where n is the number of rotors , and ς is the area of the spinning blade disc of one rotor.

The Epm can then be calculated as

$$Epm = P/v_a = \frac{\left(g\sum_{k=1}^{3} m_k\right)^{3/2}}{v_a\sqrt{2n\rho\varsigma}}. \quad (8)$$

This does not include power for avionics or an adjustment for wind or power transfer efficiency η.

Field tests conducted with the Hexa-B drone with no payload showed that hovering consumed 2.3% more power than steady flight at 6 m/s, and 4.7% more power than repeated altitude changes (vertical flight) from 0 to 25 m. Field test data while hovering with small payloads of 0.5-1.5 kg provided very different, and much larger power consumption levels than the theoretical model of eq.(7) (4.5 to 5 times larger!).

The authors also approximate the hover power consumption as a linear function of the battery and payload weight for an ArduCopter Hexa-B drone with $n = 6$, $\varsigma = 0.2$ m^2, and a frame weight $m_1 = 1.5$ kg as

$$P = \beta_1(m_2 + m_3) + \beta_0 , \quad (9)$$

where β_1 is the power consumed per kilogram of battery and package weight, and β_0 is the power required to keep the drone frame of mass m_1 in the air. Values of $\beta_1 = 46.7$ J/s-kg and $\beta_0 = 26.9$ J/s were generated from eq.(7) using linear regression with $m_2 + m_3$ ranging from 0 to 3 kg in increments of 0.001 kg. Regression parameters for eq.(9) based on the field tests with small payloads gave much larger values of β_1 and β_0, to provide

$$Epm = P/v_a = (217(m_2 + m_3) + 185)/v_a \quad (10)$$

$$Epm = P/v_a = (171(m_2 + m_3) + 187)/v_a \quad (11)$$

for a large 14.8 V battery and a small 11.1 V battery, respectively.

Stolaroff et al. (2018) provide a component model based on the fundamental forces of flight (including forces of the weight, parasite drag and induced drags) and also conduct field testing.

For a hovering rotocopter, the same power model is provided as in eq.(7). But for forward flight, Stolaroff et al. (2018) present a model for thrust

$$T = W + D = g\sum_{k=1}^{3} m_k + \frac{1}{2}\rho\sum_{k=1}^{3} C_{D_k}A_k\, {v_a}^2\,, \tag{12}$$

where the first term reflects the total drone weight and the second term is the parasite drag force, which depends on the drag coefficient C_{D_k} and the projected area perpendicular to travel A_k of each drone component (airframe, battery and payload). Note that when the drone hovers, the airspeed equals zero ($v_a = 0$) and so $T = \sum_{k=1}^{3} m_k g$, as in eq.(7).

With forward flight, or heavy wind, Stolaroff et al. (2018) use a power consumption formula adapted from Hoffman et al. (2007)

$$P = \frac{T(v_a sin\alpha + v_i)}{\eta}\,, \tag{13}$$

where α is the angle of attack (i.e., the angle of the airspeed to the drone rotor) and v_i is the induced speed, which can be found by solving (numerically)

$$v_i = \frac{g\sum_{k=1}^{3} m_k}{2n\rho\varsigma\sqrt{(v_a cos\alpha)^2 + (v_a sin\alpha + v_i)^2}}\,. \tag{14}$$

The angle of attack α is given by

$$\alpha = tan^{-1}\left(\frac{\frac{1}{2}\rho\left(\sum_{k=1}^{3} C_{D_k}A_k\right){v_a}^2}{g\sum_{k=1}^{3} m_k}\right). \tag{15}$$

For large values of α the drone may become unstable, so in practice α may be limited to maintain stable flight (Ai, 2020; DJI website, 2020). The overall energy consumption per meter is then given as

$$Epm = \frac{T(v_a sin\alpha + v_i)}{v_a \eta}\,, \tag{16}$$

with α from eq.(15) and v_i being the solution of eq.(14). Empty returns are assumed.

Stolaroff et al. (2018) consider a small quadcopter of total mass 2.57 kg, including a 0.5 kg payload (3D Robotics' Iris), and a larger octocopter of total mass 24 kg, including a 7 kg payload (Turbo Ace's Infinity 9). Field measurements consisting of 1073 flight segments with the small quadcopter in moderate winds (up to 7 m/s at random orientation to the direction of travel) are used to set some parameter values, including the power transfer efficiency $\eta = 0.7$. See Stolaroff et al. (2018) for details and all parameter values.

Stolaroff et al. (2018) also model the maximum range of a drone assuming that the drone carries the payload in one direction only (i.e., $m_3 = 0$ on the return trip). This is expressed as a function of the battery mass (m_2), battery energy capacity per kg (s_{batt}), the depth of battery discharge (γ), a battery safety factor f (assumed to be 1.2), and the energy consumption rate carrying the payload Epm_{loaded} and on the empty return $Epm_{unloaded}$

$$R = \frac{m_2 s_{batt} \gamma}{(Epm_{loaded} + Epm_{unloaded}) f} \quad . \tag{17}$$

Liu et al. (2017) provide a more comprehensive and detailed energy consumption model for small quadrotor UAVs. The model has three components: (i) induced power to maintain lift, which is a function of the thrust and the vertical drone speed, (ii) parasite power as in Stolaroff et al. (2018), and (iii) profile power to overcome the rotational drag encountered by propeller blades, which is a function of the thrust and the airspeed (see Rotaru and Todorov (2017) for related details on power requirements for helicopters).

The parasitic power is the same as in Stolaroff et al. (2018) and is given by $\sum_{k=1}^{3} \frac{1}{2} \rho {v_a}^3 C_{D_k} A_k$, although the authors do not explicitly consider the drag forces for the battery and the payload. The other two power components depend on the thrust, which is given by

$$T = \sqrt{(g \sum_{k=1}^{3} m_k - c_5 (v_a cos\alpha)^2)^2 + \left(\frac{1}{2} \rho \left(\sum_{k=1}^{3} C_{D_k} A_k\right) {v_a}^2\right)^2} \,, \tag{18}$$

where the term $g\sum_{k=1}^{3} m_k$ is the weight to be lifted, the term $c_5(v_a cos\alpha)^2$ reflects the lift generated from horizontal movements (likely to be especially important for hybrid drones with lifting surfaces), and the last term is again the parasitic drag. For a drone in steady level flight, the Epm, based on the total power from eq. (14) in Liu et al. (2017), is

$$Epm = \frac{\kappa_1}{\sqrt{2n\rho\varsigma}} \frac{T^{3/2}}{v_a} + \frac{1}{2}\rho\left(\sum_{k=1}^{3} C_{D_k} A_k\right) {v_a}^2 + c_2 \frac{T^{3/2}}{v_a}, \quad (19)$$

where the first term reflects the induced power, the second term reflects the parasitic power and the last term reflects the profile power, with parameter c_2 depending on the air density and details of the rotors (including the efficiency of converting rotor angular speed to thrust, the number of blades in each propeller, the blade chord width, drag coefficient, and length). Based on field testing, Liu et al. (2017) report that with a 1.43-kg 3DR IRIS+ quadcopter, $\kappa_1 = 0.8554$ and $c_2 = 0.3177$ $(m/kg)^{1/2}$. Note that including the profile power in the component model requires detailed decisions on the drone rotors and motors (for calculating c_2).

Liu et al. (2017) include some field tests, with the most involved having the drone with no payload ascend to 70 m, fly a horizontal rectangular loop for about 712 m, then descend and land back at the origin. Comparing the measured power and the estimated power from the proposed models shows that the model underestimated the energy consumed in ascending by 10.7%, underestimated the energy consumed in horizontal flight by 16.3%, and overestimated the energy consumed in descending by 2.2%. For the total flight, the model underpredicted the energy by 11.4%. Because the experiment was for a short flight, ascending and descending consumed 39% of the total energy; for a longer trip, ascent and descent would consume only a small part of the total energy. For the horizontal portion of the rectangular loop trip (of approximate length 712 m), the reported energy consumption is 1.23×10^4 J which equates to about $Epm = 17.3$ J/m.

Kirschstein (2020) provides a component model originally from Langelaan et al. (2017) based on an idealized delivery process (like Xu (2017)) with takeoff and ascent at 45° to a cruising altitude (150 m), level flight, descent (at 45°) with hovering, then landing for delivery. The return is similar but without the payload. Like Liu et al. (2017) the model includes energy consumed for induced power, parasite power, and profile power; but different than Liu et al. (2017), the model also includes power for climbing and avionics, and adjustments for power losses due to the electric motor and charging. For steady flight, Kirschstein (2020) uses a thrust of

$$T = \sqrt{(g\sum_{k=1}^{3} m_k)^2 + \left(\frac{1}{2}\rho\left(\sum_{k=1}^{3} C_{D_k}A_k\right){v_a}^2\right)^2} + \rho\left(\sum_{k=1}^{3} C_{D_k}A_k\right){v_a}^2 mg\sin\theta, \quad (20)$$

where the flight angle θ allows ascending and descending to be modeled. (For horizontal flight $\theta = 0$.) For hovering (with no winds), $v_a = 0$, and the thrust reduces to $g\sum_{k=1}^{3} m_k$. Kirschstein's general energy model is detailed in Appendix B and the Epm for steady level flight (i.e., $\theta = 0$) with no wind can be written as

$$Epm = \frac{1}{\eta}\left(\frac{\kappa T w}{v_a} + \frac{1}{2}\rho\left(\sum_{k=1}^{3} C_{D_k}A_k\right){v_a}^2 + \frac{\kappa_2\left(g\sum_{k=1}^{3} m_k\right)^{1.5}}{v_a} + \kappa_3\left(g\sum_{k=1}^{3} m_k\right)^{0.5} v_a\right) + \frac{P_{avio}}{\eta_c v_a}. \quad (21)$$

The first term in the Epm is for induced power with κ being the "lifting power markup" and w the "downwash coefficient" (See Kirschstein (2020) for details). The second term in the Epm is for parasite drag (as in Liu et al. (2017) and Stolaroff et al. (2018)). The third and fourth terms are for profile power where constants κ_2 and κ_3 reflect details of the rotors and environment (as in Liu et al. (2017)). The last term in the Epm is for avionics.

Kirschstein (2020) provides analyses for delivery in an urban region (comparing drones with diesel and electric trucks) with large octocopter drones (m_1+$m_2 = 12$ kg) that carry a 2.5 kg payload ($m_3 = 2.5$ kg), travel at 22.2 m/s, have a flight radius of 9 km (and the trips include 5

minutes of hovering) and $P_{avio} = 100$ J/s (as in D'Andrea (2014)). For this drone, the constants in eq.(20) are: $\kappa = 1.15$, $\kappa_2 = 0.502$ and $\kappa_3 = 0.118$; and the loaded $Epm = 131.5$ J/m.

Tseng et al. (2017a, 2017b) present a nine-term nonlinear regression model for drone power use that includes horizontal and vertical speeds and acceleration, as well as payload mass and wind speed, and provides a good fit to the reported field data. The regression model for steady flight with no wind reduces to $P = \beta_1 v_a + \beta_7 m_2 + \beta_9$. They collected data to estimate the parameters based on test drone flights using a SDR Solo drone (weighing 2 kg) with small payloads of 0 kg, 0.25 kg, and 0.5 kg, and a DJI Matrice 100 drone (weighing 2.8 kg) with small payloads of 0 kg, 0.3 kg, and 0.6 kg. The regression equation for Epm in Tseng et al. (2017b) and Tseng (2020) for steady flight with speeds up to 5 m/s and no wind for the larger DJI Matrice 100 drone is

$$Epm = \frac{P}{v_a} = -1.526 + \frac{0.220 m_2 + 433.9}{v_a}. \quad (22)$$

and for the smaller SDR Solo drone it is

$$Epm = -2.595 + \frac{0.197 m_2 + 251.7}{v_a}, \quad (23)$$

4. Analysis and results

In this section, we compare results for key drone energy models described in Section 3 to explore the interrelated aspects of payload mass, speed, energy consumption per meter and maximum drone range. The energy use and drone range are outputs determined by (i) specifics of the drone and the battery modeled, (ii) operations, specifically speed and payload mass, and (iii) environmental conditions. Table 3 summarizes the 11 drone energy models examined in this section, arranged in order of increasing drone weight.

Table 3. Key drone energy models

Color	ID	Reference	Model Type[1]	Drone Type (index)	$m_1 + m_2$ (kg)	Payload used in results (kg)	Airspeed v_a (m/s)	Equation for Epm	Field tests to set parameters
Blue	L-4-L	Liu et al. (2017)	C	Quadcopter (4)	1.46 (L)	0	8-23	(18-19)	X
Blue	S-4-L	Stolaroff et al. (2018)	C	Quadcopter (4)	2.07 (L)	0.5	10	(12-16)	X
Blue	DH-6-L	Dorling et al. (2017)	C	Hexacopter (6)	2 (L)	1	hovering	(8)	
Blue	DR-6-L	Dorling et al. (2017)	R	Hexacopter (6)	2 (L)	0 – 1	6	(10)	X
Blue	T1-4-L	Tseng et al. (2017b)	R	Quadcopter (4)	2 (L)	0 – 0.5	0-5	(22)	X
Blue	T2-4-L	Tseng et al. (2017b)	R	Quadcopter (4)	2.8 (L)	0 – 0.6	0-5	(23)	X
Blue	A-G-L	D'Andrea (2014)	I	General (G)	4 (L)	2	12.5	(4)	
Orange	F-4-M	Figliozzi (2017)	I	Quadcopter (4)	10.1 (M)	5	unknown	(5)	
Orange	K-8-M	Kirschstein (2020)	C	Octocopter (8)	12 (M)	2.5	22.2	(20-21)	
Red	S-8-H	Stolaroff et al. (2018)	C	Octocopter (8)	17 (H)	7	10	(12-16)	X
Red	X-H-H	Xu (2017)	I	Hybrid-current (H)	24.95 (H)	2.3	22.2	Not available[2]	

[1]C = component model; R = regression model; I = integrated model

[2]based on D'Andrea (2014)

Columns 1-2 provide the color and ID used in later figures. The first part of the ID (1 or 2 characters) indicates the reference and model, where DH and DR respectively indicate the theoretical hovering model and the regression model in Dorling et al. (2017), and T1 and T2 indicate the two regression models from Tseng et al. (2017b). The second part of the ID is the number of rotors for the drone or the drone type. The third part of the ID indicates the drone size, with "L" for light drones (<4 kg), "M" for medium drones (4-15 kg) and "H" for heavy drones (>15 kg). Note that the majority of models are for small rotocopter drones with small payloads. Column 3 identifies the reference. Column 4 describes the model type (integrated, component or regression) as discussed in Section 3. Columns 5-8 provide information on the drone type, mass and airspeed as described in the reference. Column 9 is the equation number in this paper for Epm. Column 10 indicates if parameters in the equation were set based on field experiments with a particular drone. Each article in Table 3 provides at least one data point for Epm based on a particular drone model in steady flight, with the regression models providing multiple data points.

4.1 Epm results from the literature

Figure 3 shows a graph of Epm versus payload mass for the models in Table 3. There are three short lines for the regression models (DR-6-L, T1-4-L, T2-4-L), two points each for the D'Andrea and Kirschstein models, and one point each for the other six models. For the D'Andrea (2014) and Kirschsteain (2020) models, the lower point (A-G-L or K-8-M) is the base model for steady level flight with no wind or avionics, while the upper point (A-G-L++ and K-8-M++) includes a 10 m/s headwind and avionics to show the impact of additional power requirements. As expected, the general trend is for larger payloads to have larger Epm values; however, the range of Epm values varies substantially, both across the payloads and for similar payloads. The models for light drones with payloads of ≤1 kg cluster in the lower left of Figure 3, with Epm values

ranging from 16 J/m for DH-6-L to 107 J/m for T2-4-L. The Epm for drones with payloads of 2-5 kg range from 39 J/m for A-G-L to 168 J/m for X-H-H, though it should be noted that the values reported for X-H-H include a complete delivery mission with ascent, descent, hovering and headwind. When including the impact of wind and avionics, the A-G-L++ and K-8-M++ models provide Epm values of 141 J/m and 203 J/m, which are substantial increases over the Epm for A-G-L (262%) and K-8-M (73%), respectively. The S-8-H model for the drone with the largest payload (7 kg) provides by far the largest Epm of 436 J/m, which is 2.5 times larger than the energy for the other "heavy" drone X-H-H model, though the latter is with a much smaller 2.3 kg payload.

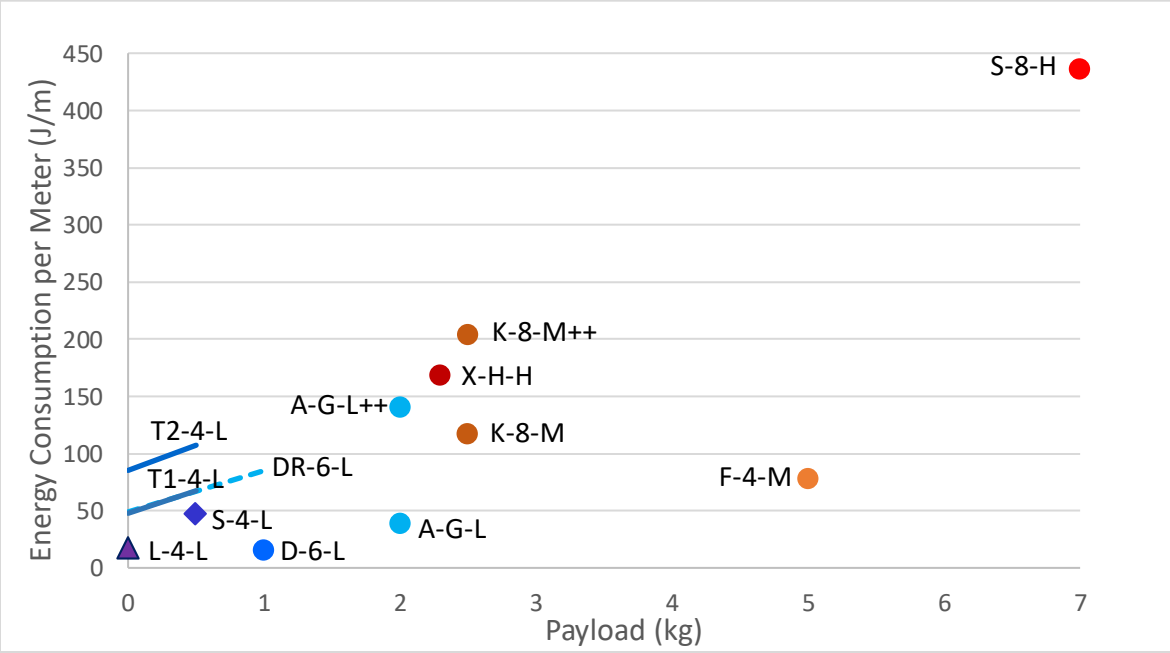

Figure 3. Epm results from models in the literature

Key findings revealed by Figure 3 are: (i) the energy consumption for steady level flight varies substantially with the payload for the models in the literature, from under 20 J/m to over 400 J/m for payloads up to 7 kg; (ii) with similar payloads the energy consumption models differ

by factors of several hundred percent; and (iii) including factors beyond steady level flight (e.g., wind, avionics, hovering, a complete delivery cycle, etc.) greatly increases energy requirements – (over 100%) for some models (see also Kirschstein (2020) for more details).

Figure 3 displays Epm values from the models or field tests described in the corresponding articles, but we note that these could be used for other delivery settings, such as delivering lighter payloads. For example, using the Stolaroff et al. (2018) heavy drone S-8-H model with a small 2 kg payload would reduce the Epm to 322 J/m, which is still well above the values reported for the other models with similar payloads. Not shown in Figure 3 are some hypothesized future drones, where the Epm is predicted to be considerably reduced due to developments in technology and improved drone designs. For example, the future drone described in Xu et al. (2017) incorporates efficiencies that reduce Epm by 83% (from 168 J/m to 29 J/m) and the future drone in Figliozzi (2017) reduces Epm by 50%.

In summary, Figure 3 highlights the lack of agreement on drone energy consumption rates in the published literature. Sources of these disagreements stem from the different types of drones modeled (e.g., different sizes, drag coefficients, motor and rotor details, power transfer efficiencies, etc.), the different components of the power included in the models, different operating conditions (speed, payload, wind, etc.), and different operating settings (values for air density, gravity acceleration, empty returns, etc.). However, we note that with the same operating settings and parameters the different drone models also produce quite different results.

4.2 Results for different modeling approaches with a common drone and operational setting

To assess the drone energy consumption models from the literature on a common basis, we evaluate five fundamental modeling approaches discussed in Section 3 using common drone design parameters and a common operational setting, where the payload and speed are allowed to

vary. The modeling approaches are identified in Table 4, along with the key reference and the equation(s) for Epm. The first model, denoted LD, is the integrated model with a lift-to-drag ratio, based on eq.(4) from D'Andrea (2014). The second model, denoted RH, includes the energy use for rotocopter hovering only, as in eq.(8) from Dorling et al (2017). The third model, denoted R2, includes two rotocopter energy components to overcome the induced drag and parasite drag, as in Stolaroff et al. (2018). The fourth model, denoted R3, includes three rotocopter energy components, as it adds the profile drag to the induced and parasite drag, as in Kirschstein (2020). The final model, denoted LR, is the regression model from Tseng (2017b) that provides Epm as a function of payload mass and airspeed.

To compare the models on a common basis we fix the environmental parameters (e.g., gravity, air density, etc.) to the common values shown in Table C.1 in Appendix C. To model both large and small drones, we use the different parameters values shown in Table C.2 in Appendix C, based on the values from Stolaroff et al. (2018). For all models, we include a common value for the power transfer efficiency, and we assume empty returns so the Epm values in this section are the average of the loaded (with the payload) and unloaded (without the payload) Epm values. We consider a setting with no wind, and do not include energy for avionics, vertical flight or hovering (though these may add substantially to the energy requirements). We vary either the payload mass or the airspeed to explore their effects on Epm and range. Thus, by using the same drone specification and flight conditions, we can document the variability due to the different model structures and assumptions (not due to different input data). The performance measures of interest are Epm and flight range. Range is calculated from eq. (17) based on the Epm calculated using the equations in Table 4.

Table 4. Five fundamental models for drone energy consumption of steady level flight

Model	Key Reference	Epm
LD	D'Andrea (2014)	$\frac{\sum_{k=1}^{3} m_k g}{r\eta}$
RH	Dorling et al. (2017)	$\frac{(\sum_{k=1}^{3} m_k\, g)^{3/2}}{\eta v_a \sqrt{2n\rho\varsigma}}$
R2	Stolaroff et al. (2018)	$\frac{T(v_a sin\alpha + v_i)}{v_a \eta}$ where $T = g\sum_{k=1}^{3} m_k + \frac{1}{2}\rho \sum_{k=1}^{3} C_{D_k} A_k\, {v_a}^2$ and v_i is found from solving equations (14-15)
R3	Kirschstein (2020)	$\frac{1}{\eta}\left(\frac{\kappa T w}{v_a} + \frac{1}{2}\rho \sum_{k=1}^{3} C_{D_k} A_k\, {v_a}^2 + \frac{\kappa_2 (\sum_{k=1}^{3} m_k\, g)^{1.5}}{v_a} + \kappa_3 \left(\sum_{k=1}^{3} m_k g\right)^{0.5} v_a\right)$ where $T = \sqrt{(\sum_{k=1}^{3} m_k g)^2 + \left(\frac{1}{2}\rho \sum_{k=1}^{3} C_{D_k} A_k\, {v_a}^2\right)^2}$ and w is from solving equation (B2)
LR	Tseng (2017b)	$-2.595 + \frac{0.197 m_2 + 251.7}{v_a}$ (for small payloads and speeds less than 5 m/s)

4.2.1 Results for small drones

In the small drone case, the delivery setting is a small quadcopter drone able to carry a payload up to 0.5 kg with the parameter values in Tables C.1 and C.2. We begin by examining the effect on Epm of changes in the payload. Figure 4 shows for all models an approximately linear increase in Epm with increased payload. Model LD provides the lowest Epm values of about 10 J/m, with the RH model giving values about twice as large. The R2 and LR models give similar results, about 2.5 times the LD results. The largest Epm comes from the more comprehensive R3

model, where Epm is 32-39 J/m. Note that a smaller lift-to-drag ratio in the LD model would provide very similar results to the other models, which implies that the LD model with $r = 3$ is a more efficient drone than the others. The high energy consumption for the R3 model is in part due to it including the profile drag, while using the same power transfer efficiency ($\eta = 0.7$) as the other models. So, modelers could use a lower power transfer efficiency to reflect modeling of fewer components of power (e.g., a lower η value could be used in R2 compared to R3 for not including the profile power directly in R2).

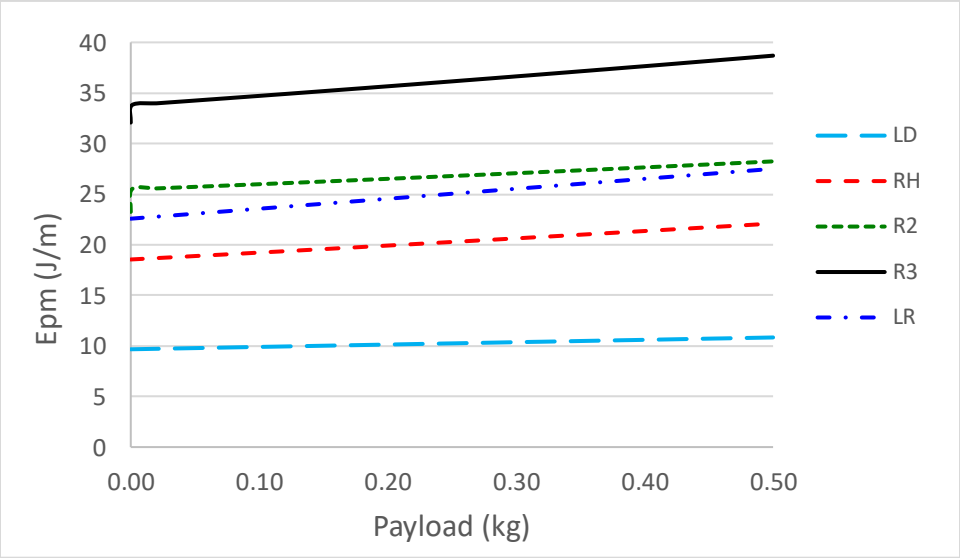

Figure 4. Energy consumption rate versus payload for small drones.

Overall, Figure 4 shows the very wide variation in Epm values for different modeling approaches (differing by a factor of 3!) with the same drone operating in a common setting. These differences have strong implications for accurately modeling the energy and assessing the environmental impacts of drone delivery. These results also indicate that the selection of the lift-to-drag ratio r and the power transfer efficiency η, both of which are difficult to assess without taking measurements in flight, can be crucial in accurately estimating drone energy consumption.

Figure 5 shows the maximum one-way drone flight range for the five models as a function of the payload for the small drones. As expected, the flight range decreases for all models as payload increases. The range decreases vary from 1.3 km (11%) for LD to 0.6 km (17%) for R3 when moving from no payload to 0.5 kg. The LD model provides the largest range of 10-12 km, and the other four models produce smaller ranges between 3-6 km, which are 28-50% of the range of the LD model. As with Epm, a smaller lift-to-drag ratio in the LD model, with r between 1.5 and 0.9 instead of 3, would produce range results between the lower limit from R3 and the upper limit from RH. As with Epm, the results show the large variability in ranges for the different models, and this has clear implications of the number of customers that could be served by drone, and the number of drone depots needed to serve a region.

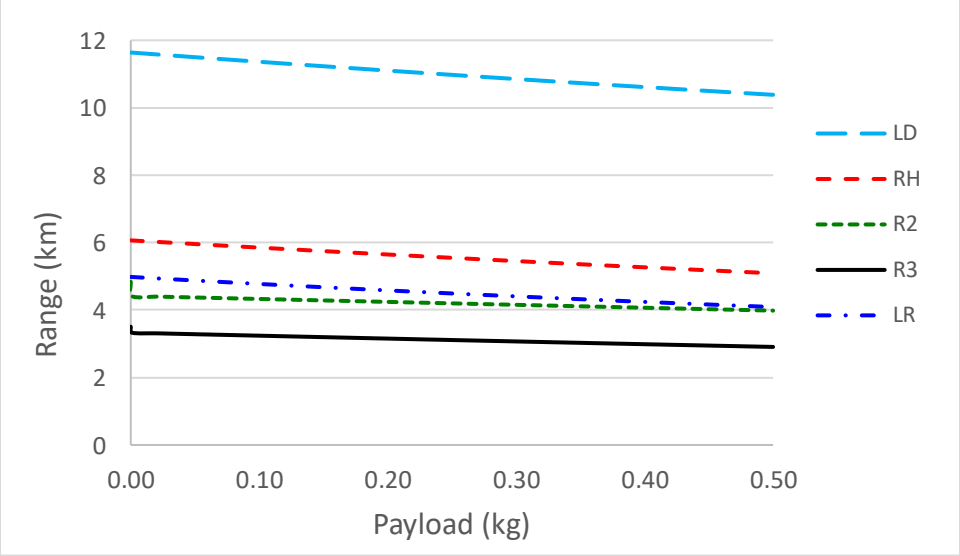

Figure 5. Maximum range for small drones with payload varying from 0.0-0.5 kg

Next, we consider the same small drone models, but we fix the payload at 0.5 kg and allow the airspeed to vary from 1-25 m/s. Results for energy consumption and range are shown in Figures 6 and 7, respectively. The LR model is shown only for speeds from 1-5 m/s as that is the relevant

range for the regression (Tseng, 2017b). Note that Epm with the LD model does not change with speed as it assumes the lift-to-drag ratio is constant. For all other models, the Epm is a decreasing function of airspeed for low speeds, with R3 providing the highest Epm and RH and R2 providing nearly identical lowest Epm values (R2 and RH are remarkably similar for speeds up to 8 m/s). Epm is a convex function of airspeed for the component models R2 and R3, as overcoming the parasite drag at high speeds requires a large increase in energy.

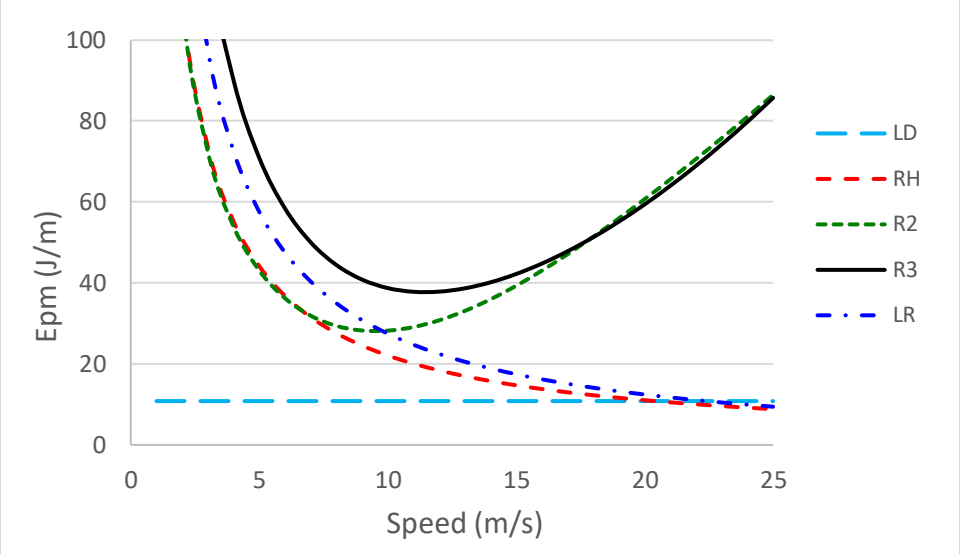

Figure 6. Energy consumption rate versus airspeed for small drones.

We note that the Epm is relatively flat around the energy-minimizing speed for the R2 and R3 models, which is about 10-11 m/s, though the minimum Epm value for R3 (37.8 J/m) is one-third larger than that for R2 (28.2 J/m). For models other than the LD model, the Epm is more sensitive to lower speeds than higher speeds; and while the models all have similar shapes for low speeds, they may produce very different values. For example, at 5 m/s the Epm values for the 4 models range from 43 J/m for R2 to 71 J/m for R3. The differing nature of the RH model (based on hovering) is clear as with higher speeds its Epm continues to decline as it is unable to capture the effect of increasing air resistance. As noted above, the LD model uses much less energy, though

adjusting the lift-to-drag ratio r to a value 0.8-1.1 would make LD model produce results similar to the energy-minimizing values for the R2 and R3 models.

Figure 7 shows the drone flight range versus airspeed for the five models. As with Epm, the range for the LD model does not change with speed, and is 10.4 km. The range for the RH and LR models is linearly increasing in speed. The range for the R2 and R3 models follows a more complex pattern reflecting the convex Epm graphs. The maximum range for the R2 and R3 models (which occurs with the energy-minimizing speed) is about 4 km and 3 km, respectively, less than half the range from the LD model.

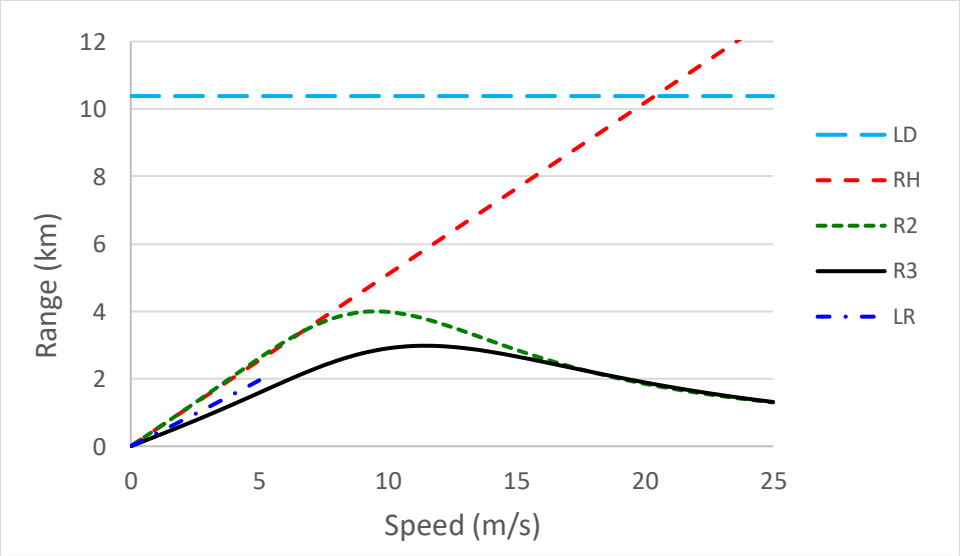

Figure 7. Maximum flight range versus airspeed for small drones.

We note that slower speeds quickly increase energy consumption, and the range for all models (except LD) falls quickly for slow drone speeds. For speeds below about 9 m/s, the four models other than the LD model provide similar short ranges. Note that these ranges are based on a small drone with a 1 kg battery of specific energy 540,000 J, with a 70% battery transfer efficiency, a 20% safety factor (to reserve energy for unusual conditions) and a 50% depth of

battery discharge (see Table C.1). Having a larger, more efficient or more energy dense battery would increase the range. However, because the calculated range values do not include any energy for hovering, takeoff and landing or ascending and descending, the actual range would be less than that calculated based purely on steady level flight (see Kirschstein, 2020; Xu, 2017).

4.2.2 Results for large drones

This section considers the same analyses as above but for a large drone able to carry payload up to 7 kg. For the LD model we retain the lift-to-drag ratio of $r = 3$ from D'Andrea (2014). Because the LR regression model in Tseng et al. (2017b) was developed specifically for a small drone, we do not include that model in this section. Figures 8-11 provide results for the large drone energy consumption and flight range with models LD, RH, R2 and R3, similar to Figures 4-7 for the small drone.

Figure 8 shows the Emp versus payload results for the large drone with payloads up to 7 kg. As for the small drone, the Epm increases linearly with payload, the LD model provides the lowest Epm (80-96 J/m); the R3 model provides the largest Epm (over 400 J/m), about 5 times larger than that from the LD model; and the RH and R2 models provide very similar performance in between the other models, and about 2-2.5 times the LD result. The Epm increases by 22-43% for the four models as the payload rises from 0 to 7 kg. The results show that using these large drones with small payloads requires about 6 times (for R2) to 11 times (for R3) as much energy as using the corresponding model for a small drone (shown in Figure 4). The increased Epm is mainly due to the increased drone weight (including battery), which shows the importance of using an appropriate drone for the items (and purpose of delivery). Overall, the results for large drones (Figure 8) behave similarly to those for small drones (Figure 4), although the Epm of R3 model is relatively much larger for the large drones.

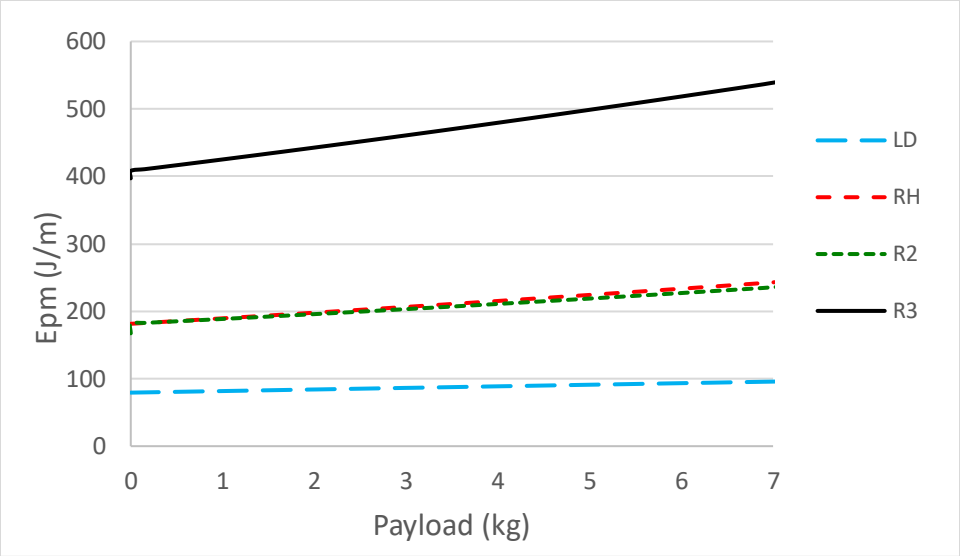

Figure 8. Energy consumption rate versus payload for large drones.

Figure 9 provides results for the flight range from the four large drone models for payloads from 0-7 kg. As expected, the drone range decreases with all models as the payload increases, with a decline of 18-30% (2.5-0.7 km) when moving from no payload to 7 kg. The LD model provides the largest range of 11.6-14.1 km, and the R3 model provides the smallest range (2.1-2.8 km). In comparison to the small drone, the large drone has a battery that is ten times larger, while the total drone weight (with battery and payload) is about 8-9 times larger (than for the small drone) depending on the payload. Results show the range values for the large drone are: (i) very similar to those for the small drone, as with the RH model; (ii) 20-40% greater than for the small drone, as with the R2 model; or (iii) 20-30% smaller than for the small drone, as with the R3 model.

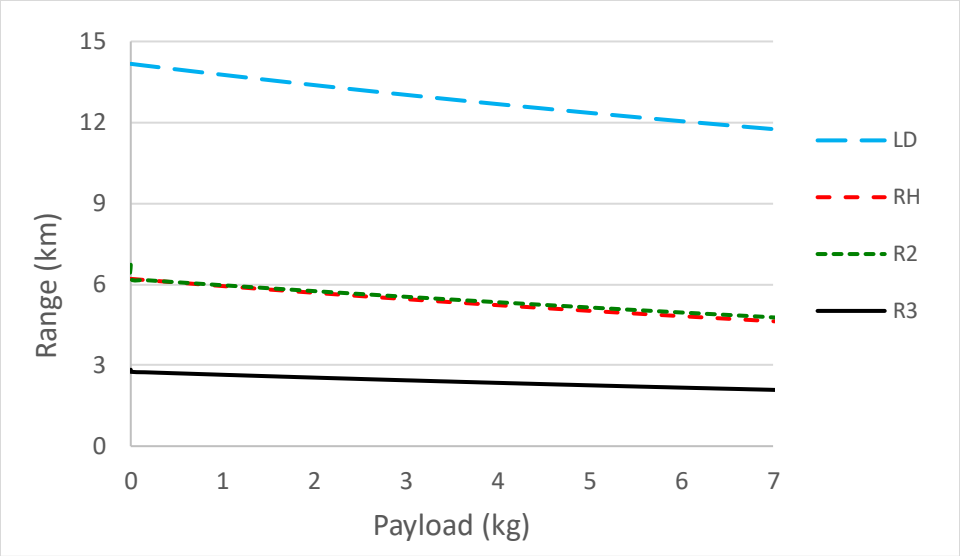

Figure 9. Range versus payload for large drones.

Figures 10-11 show the large drone Epm and range as a function of the airspeed, with the payload fixed at 7 kg. Most findings are similar to the small drone. The shapes of the curves for the large drone Epm are similar to those for the small drone (Figure 6), though the curves are less steep for large drones, and at higher speeds the Epm for model R3 remains above R2 with the large drone. As for the small drone, RH and R2 provide nearly identical lowest Epm values up to the energy-minimizing speed for R2 (about 12 m/s). The convex shapes for R2 and R3 clearly show the large parasite drag at high speeds.

Again the Epm is relatively flat around the energy-minimizing speed for the R2 and R3 models, which is about 13 m/s for R2 and 16 m/s for R3 (greater values than for the small drone). At this energy-minimizing speed, the Epm for the R3 model is about twice as large as for the R2 model (416 J/m vs 212 J/m), which is a considerably larger relative difference than with the small drone. Except for the similarity of R2 and RH (below 12 m/s), the Epm values for the different models differ dramatically. For example, at 5 m/s the Epm values range from 96 J/m for LD, 467-

486 for R2 and RH, to 1090 for R3; at 10 m/s the Epm values range from 96 J/m for LD, 235-243 for R2 and RH, to 539 for R3. Again, we note that the LD model uses much less energy, though adjusting the lift-to-drag ratio r would produce results similar to the energy-minimizing values for the R2 and R3 models.

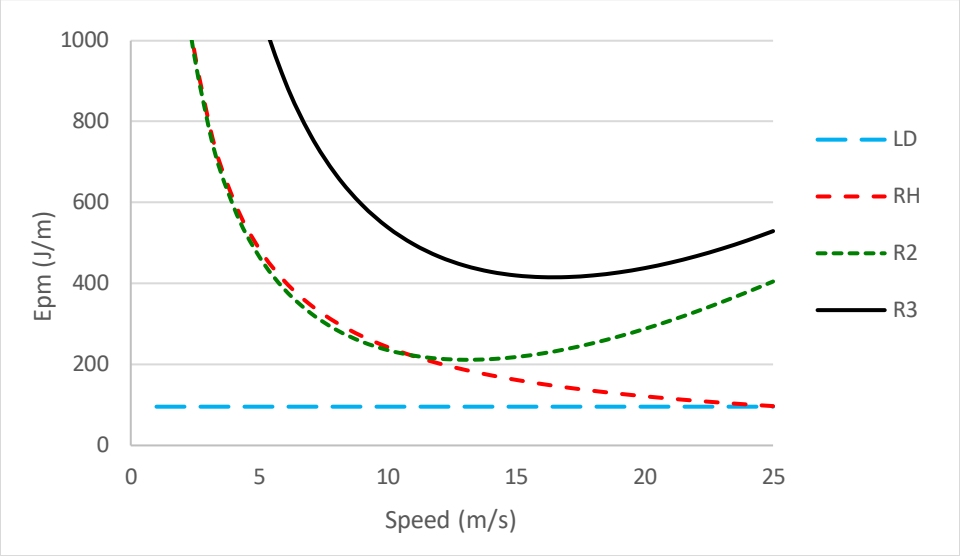

Figure 10. Energy consumption rate versus airspeed for large drones.

Figure 11 provides flight range versus speed results for the large drone with the 7 kg payload. The results are qualitatively similar to those for the small drone (Figure 7). The flight range for the LD model increases slightly to 11.8 km (vs 10.4 km for the small drone). The flight range for the R2 and R3 models both increase relative to the range for the small drone, from 2.7 km to 5.4 km for R2 and from 3 km to 4 km for R3.

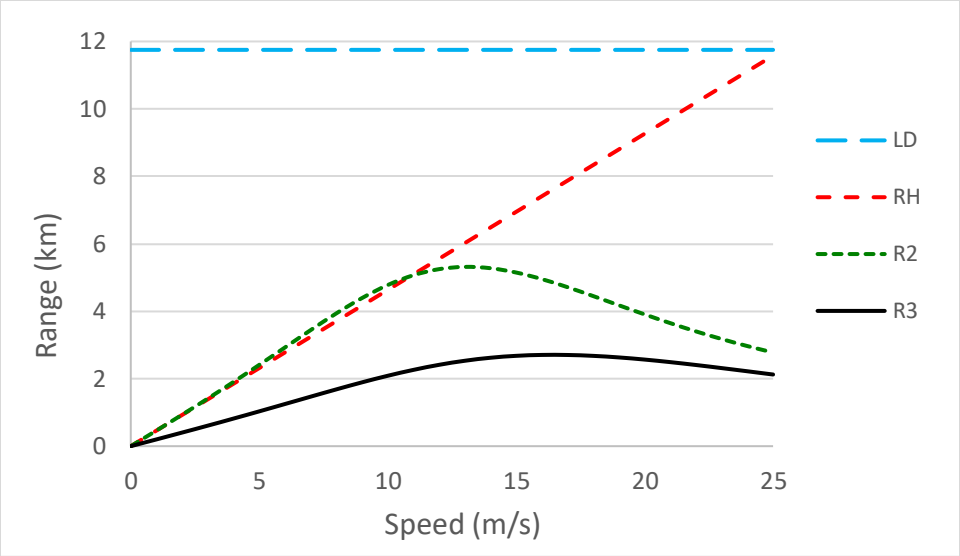

Figure 11. Maximum flight range versus airspeed for large drones.

5. Discussions and insights

The results in this paper demonstrate very large differences in drone energy consumption rates and operating ranges derived from different models in the literature. Some of the reported results differ due to different drone types and different operating conditions. However, even with a common setting that uses the same drone design and operating parameters, the models provide Epm and range estimates for steady level flight that differ substantially. Further, we note that when a full drone delivery flight profile is included (with takeoff, ascent, hovering, descent, and landing phases), the Epm values can be substantially higher than the results for the steady level flight alone. Key findings from this research include:

- There are several fundamentally different approaches for modeling drone energy consumption, including integrated approaches reliant on a lift-to-drag ratio to capture performance, component models developed to capture the influence of key aerodynamic forces, and regression models calibrated from field tests or from theoretical models.

- For published models, the energy consumption rate (Epm) for steady level delivery drone flight ranges from 16 J/m to over 400 J/m for different types of drones with different payloads. Even for small drones with payloads up to 1 kg, the literature provides Epm values that differ by a factor of six. Note that many of these Epm values reflect off-the-shelf drones (for both theoretical modeling and field experiments), not drones designed specifically for package delivery, and thus may not reflect actual drone delivery operations.
- To better assess fundamental drone energy models, we use a common set of environment and drone design and operating parameters for models of both large and small drones. Even with the common sets of parameters, the energy consumption rate (Epm) varies by a factor of 3-5 across the models (see Figures 4, 6, 8 and 10). The estimated drone flight ranges differ similarly for the models.
- Integrated models (like the LD model) have the appeal of simplicity, but are very sensitive to the choice of the lift-to-drag ratio and do not vary with airspeed. Thus, only with a properly calibrated lift-to-drag ratio (ideally based on field experiments in the relevant setting) and operating airspeed will they provide accurate estimates of energy consumption.
- Models based only on energy consumption for drone hovering (like the RH model) may provide very good approximations at low airspeeds. However, at higher speeds they cannot capture the increased parasite drag that grows to dominate the energy consumption.
- Component models provide the most detail, but are the most difficult to develop and calibrate given the number of parameters involved. Component models capture the strong dependence of Epm and range on airspeed, and allow identification of an energy-minimizing airspeed. The two-component model (R2) and a three-component model (R3) highlighted the differences from modeling profile power directly and the importance of using a proper power transfer

efficiency adjustment. All drone energy models include a power transfer adjustment to reflect losses due to a variety of sources, including battery charging efficiency, motor efficiency, drone blade performance, etc.; so it would be natural for a two component model to include a lower power transfer efficiency than a three component model to reflect power losses from the "missing" component. Our use of a common power transfer efficiency may explain in part the lower energy consumption for the R2 vs. R3 model.

- Published results for energy consumption from drone field tests, sometimes with drone actions other than steady level flight, often do not agree with results from theoretical energy models. There is growing evidence about the need to account for the energy used in the entire drone delivery cycle (takeoff, ascent, hovering, descent, landing, and return), as well as for avionics and for wind conditions to accurately estimate total energy consumption of delivery drones. The models used by Kirschstein (2020) and Xu (2017) are good examples.
- There is a strong need for more field experiments to estimate parameter values (or reasonable ranges for these values) for modeling various drone types, including new hybrid drones. The goal, as the drone delivery industry matures, is to develop sets of commonly agreed parameter values for effective delivery drones (just as exist for commercial aircraft) to use in research on optimizing the design and operation of drone delivery systems.

6. Conclusions

In this study, we provide a review of key energy consumption models for drone delivery. We identify the important factors that influence drone energy consumption, and discuss and highlight key similarities and differences in drone energy models. We also provide an understanding of why the energy consumption models differ from each other, and identify key parameters. The selection of the lift-to-drag ratio r and the power transfer efficiency η, both of

which are difficult to assess without taking measurements in flight, can be crucial in accurately estimating energy consumption for drones.

The energy consumption differences we document have strong implications for accurately modeling the energy and environmental implications of drone delivery. Given that the models provide Epm values that differ by a factor of 3-5 (or more), great care must be taken in translating results from transportation modeling (e.g., drone route modeling and optimization) to estimates and policy recommendations involving energy and emissions. The mixed research results regarding the energy and emissions efficiency of drone delivery is not surprising given the wide variability in energy consumption estimates produced from different Epm models. Research has shown that the emissions benefits of drones relative to trucks strongly depend on the drone energy consumption rate (Goodchild and Toy, 2018); however the highest energy consumption rate used in Goodchild and Toy is considerably below the rate from Kirschstein (2020) and the R3 model.

Our goal is not to identify one preferred model, but rather to document the discrepancies between models and highlight the need for accurate parameter values in whatever model is adopted. All models examined in this paper can produce similar results with an appropriate set of parameter values. Given the lack of widespread drone delivery operations that prevent direct measurements in the field, it is not surprising there is no agreement on accurate parameter values in the academic research community. Further, with the rapid rate of evolution in drone technology, those parameter values will likely change frequently as the field matures.

This research suggests a number of important areas for future research. Clearly, a better understanding of the accuracy of drone energy models is needed through comparing results to empirical data from comprehensive drone delivery field tests. The importance of avionics and wind conditions on drone energy consumption is an area especially needing more attention. Different

drone delivery operations will likely use quite different drones, such as for delivery of small amounts (<0.5 kg) of medical items (samples, medications, etc.) in a controlled environment versus delivery of consumer goods (up to 5 kg) to homes. Thus, while a particular drone model might be effective in both cases, it would necessarily need very different parameter values to be accurate in multiple settings. Future research can also help identify which type of model is best in different settings, and whether or when more parsimonious models are "accurate enough" to use.

As energy consumption connects to both cost and emissions, an important broad research area is to better link drone energy models with route optimization and strategic drone delivery system design to assess the tradeoffs between cost, energy, and emissions in drone delivery. For drones, the role of airspeed, as well as wind conditions, has a very important influence on energy consumption, more so than for trucks and other ground delivery vehicles, and should also be included. This also has implications for combined truck-drone delivery systems where synchronizing the truck and drone arrival at docking locations is required.

References

Adams E., 2016. DHL's Tilt-Rotor 'Parcelcopter' is both awesome and actually useful. *WIRED*. Retrieved January 23rd, 2020 from: https://www.wired.com/2016/05/dhls-new-drone-can-ship-packages-around-alps/.

Agatz, N., Bouman, P. and Schmidt, M., 2018. Optimization approaches for the traveling salesman problem with drone. *Transportation Science*, *52*(4), 965-981.

Ai S., 2019. Personal communication, December 1st, 2019.

Chauhan, D., Unnikrishnan, A. and Figliozzi, M., 2019. Maximum coverage capacitated facility location problem with range constrained drones. *Transportation Research Part C: Emerging Technologies*, *99*, pp.1-18.

Chiang, W. C., Li, Y., Shang, J. and Urban, T. L., 2019. Impact of drone delivery on sustainability and cost: Realizing the UAV potential through vehicle routing optimization. *Applied energy*, *242*, 1164-1175.

Cohen, J. K., 2019. WakeMed Health & Hospitals joins forces with UPS, FAA for drone pilot. *Modern Healthcare*. Retrieved January 23rd, 2020 from: https://www.modernhealthcare.com/care-delivery/wakemed-health-hospitals-joins-forces-ups-faa-drone-pilot.

D'Andrea, R., 2014. Guest editorial can drones deliver?. *IEEE Transactions on Automation Science and Engineering*, *11*(3), 647-648.

Demir, E., Bektaş, T., and Laporte, G., 2014. A review of recent research on green road freight transportation. *European Journal of Operational Research*, *237*(3), 775-793.

Di Franco, C. and Buttazzo, G., 2015. Energy aware coverage path planning of UAVs, 2015 IEEE International Conference on Autonomous Robot Systems and Competitions. https://ieeexplore.ieee.org/stamp/stamp.jsp?tp=&arnumber=7101619

DJI website (2020), https://www.dji.com/phantom-4-pro-v2/specs retrieved May 3rd, 2020

Dorling, K., Heinrichs, J., Messier, G. G., and Magierowski, S., 2017. Vehicle routing problems for drone delivery. *IEEE Transactions on Systems, Man, and Cybernetics: Systems*, *47*(1), 70-85.

Drones in HealthCare. A Role for Drones in Healthcare. Retrieved January 23rd, 2020 from its website: https://www.dronesinhealthcare.com/

Ferrandez, S.M., Harbison, T., Weber, T., Sturges, R. and Rich, R., 2016. Optimization of a truck-drone in tandem delivery network using k-means and genetic algorithm. *Journal of Industrial Engineering and Management (JIEM)*, *9*(2), pp.374-388.

Figliozzi, M. A., 2017. Lifecycle modeling and assessment of unmanned aerial vehicles (drones) CO 2 e emissions. *Transportation Research Part D: Transport and Environment*, *57*, 251-261.

Filippone, A., 2006. Flight performance of fixed and rotary wing aircraft. Washington, DC, USA: AIAA, 2006.

Goodchild, A. and Toy, J., 2018. Delivery by drone: An evaluation of unmanned aerial vehicle technology in reducing CO_2 emissions in the delivery service industry. *Transportation Research Part D: Transport and Environment*, *61*, 58-67.

Gulden, T. R., 2017. The energy implications of drones for package delivery. RAND Corporation, Santa Monica, CA.

Heath N., 2018. Project Wing: A cheat sheet on Alphabet's drone delivery project. Retrieved January 23rd, 2020 from: https://www.techrepublic.com/article/project-wing-a-cheat-sheet/.

Hoffmann, G., Huang, H., Waslander, S., and Tomlin, C., 2007. Quadrotor helicopter flight dynamics and control: Theory and experiment. In *AIAA Guidance, Navigation and Control Conference and Exhibit* (p. 6461).

Hong, I., Kuby, M. and Murray, A.T., 2018. A range-restricted recharging station coverage model for drone delivery service planning. *Transportation Research Part C: Emerging Technologies*, *90*, pp.198-212.

Jeong, H. Y., Song, B. D., and Lee, S., 2019. Truck-drone hybrid delivery routing: Payload-energy dependency and No-Fly zones, *International Journal of Production Economics* 214 (2019) 220–233.

Josephs L., 2019. UPS wins first broad FAA approval for drone delivery. *CNBC*. Retrieved January 23rd, 2020 from: https://www.cnbc.com/2019/10/01/ups-wins-faa-approval-for-drone-delivery-airline.html.

Kirchstein, T., 2020. Comparison of energy demands of drone-based and ground-based parcel delivery services. *Transportation Research Part D: Transport and Environment* 78, 1-18. https://doi.org/10.1016/j.trd.2019.102209

Kitjacharoenchai, P., Min, B-C. and Lee, S., 2020. Two echelon vehicle routing problem with drones in last mile delivery. *International journal of Production Economics* 225, 107598.

Langelaan, J.W., Schmitz, S., Palacios, J., and Lorenz, R.D., 2017. Energetics of rotary-wing exploration of titan. In: Aerospace Conference, 2017 IEEE, pages 1–11. IEEE.

Lee, D., 2019. Amazon to deliver by drone 'within months'. Retrieved July 12th, 2019 from: https://www.bbc.com/news/technology-48536319.

Leishman, J. G., 2002. Principles of helicopter aerodynamics (Vol. 12). Cambridge University Press.

Liu, Y., 2019. An optimization-driven dynamic vehicle routing algorithm for on-demand meal delivery using drones. *Computers & Operations Research*, *111*, pp.1-20.

Liu, Z., Sengupta, R., and Kurzhanskiy, A., 2017. A power consumption model for multi-rotor small unmanned aircraft systems. In *2017 International Conference on Unmanned Aircraft Systems (ICUAS)* (pp. 310-315). IEEE.

Lohn, A. J., 2017. What's the buzz? The city-scale impacts of drone delivery (No. RR-1718-RC).

Murray, C. C., and Chu, A. G., 2015. The flying sidekick traveling salesman problem: Optimization of drone-assisted parcel delivery. *Transportation Research Part C: Emerging Technologies*, *54*, 86-109.

Murray, C. C., and Raj, R., 2020. The multiple flying sidekicks traveling salesman problem: Parcel delivery with multiple drones. *Transportation Research Part C: Emerging Technologies*, *110*, 368-398.

Otto, A., Agatz, N., Campbell, J., Golden, B. and Pesch, E., 2018. Optimization approaches for civil applications of unmanned aerial vehicles (UAVs) or aerial drones: A survey. *Networks*, *72*(4), pp.411-458.

Poikonen, S. and Golden, B., 2020. Multi-visit drone routing problem. *Computers & Operations Research*, *113*, pp.104-802.

Rotaru, C. and Todorov, M., 2017. Helicopter flight physics, DOI: 10.5772/intechopen.71516, https://www.intechopen.com/books/flight-physics-models-techniques-and-technologies/helicopter-flight-physics

Schermer, D., Moeini, M. and Wendt, O., 2019. A hybrid VNS/Tabu search algorithm for solving the vehicle routing problem with drones and en route operations. *Computers & Operations Research*, *109*, pp.134-158.

Shavarani, S.M., Nejad, M.G., Rismanchian, F. and Izbirak, G., 2018. Application of hierarchical facility location problem for optimization of a drone delivery system: a case study of Amazon prime air in the city of San Francisco. *The International Journal of Advanced Manufacturing Technology*, *95*(9-12), pp.3141-3153.

Stolaroff, J. K., Samaras, C., O'Neill, E. R., Lubers, A., Mitchell, A. S., and Ceperley, D., 2018. Energy use and life cycle greenhouse gas emissions of drones for commercial package delivery. *Nature communications*, *9*(1), 409.

Swoop Aero, 2019. Drones for medical deliveries: the value of using technology for good. Retrieved January 23rd, 2020 from: https://swoop.aero/2019/10/21/drones-technology-for-good/.

Troudi, A., Addouche, S. A., Dellagi, S., and Mhamedi, A., 2018. Sizing of the drone delivery fleet considering energy autonomy. *Sustainability*, *10*(9), 3344.

Tseng, C-M., Chau, C-K., Elbassioni, K. and Khonji, M., 2017a. Flight Tour Planning with recharging optimization for battery-operated autonomous drones, 29 March 2017, https://pdfs.semanticscholar.org/76d2/307395999118ca3fb406c1d95e337bf3953b.pdf

Tseng, C-M., Chau, C-K., Elbassioni, K. and Khonji, M., 2017b. Autonomous recharging and flight mission planning for battery-operated autonomous drones, 12 September 2017, https://arxiv.org/pdf/1703.10049.pdf

Tseng, C-M., 2020. Personal communication , January 22 and 25, 2020.

Wu, F., Yang, D., Xiao, L. and Cuthbert, L., 2019. Energy consumption and completion time tradeoff in rotary-wing UAV enabled WPCN, IEEE Access 7, 79617-79635,10.1109/ACCESS.2019.2922651

Xu, J., 2017. Design perspectives on delivery drones. RAND.

Zeng, Y. and Zhang, R., 2017. Energy-efficient UAV communication with trajectory optimization. *IEEE Transactions on Wireless Communications*, *16*(6), 3747-3760.

Zeng, Y., Xu, J. and Zhang, R., 2019. Energy minimization for wireless communication with rotary-wing UAV. *IEEE Transactions on Wireless Communications*, *18*(4), 3747-3760.

Appendix A

This appendix provides a derivation of the energy consumption for a battery powered aircraft in steady level flight (i.e. at a constant altitude and constant speed), as in D'Andrea (2014), based on fundamental principles of flight. Four fundamental forces acting on an aircraft in steady flight are thrust to move forward, weight from gravity acting on the aircraft mass, lift in the direction opposing gravity, and drag in the direction opposing travel (from aerodynamic effects of the shape of the aircraft, such as friction with air). The amount of energy in joules needed to fly a distance d (measured in meters) at constant altitude can be modeled as

$$E_{fly} = T \times d \ , \tag{A1}$$

where T is the thrust force measured in Newtons (kg-m/sec^2). Note that this does not account for the energy involved with the vertical travel components to lift the aircraft from the ground to a cruising altitude and to lower it back to the ground. For drone delivery, this may occur twice each trip, once at takeoff/landing and once for the delivery; however, drone deliveries may not require landing, as the package may be lowed via a tether or dropped via parachute.

An important factor for aircraft performance is the lift-to-drag ratio r, a unitless parameter which captures the efficiency of the aircraft design in keeping the aircraft airborne. Values of the lift-to-drag ratio range widely from about 10-20 for commercial passenger aircraft to about 4 for helicopters in cruising flight, to typically smaller values for UAV rotocopters. The lift-to-drag ratio varies with aircraft speed due to drag and the aerodynamic affects from lifting surfaces, but is constant in steady flight. To keep the aircraft in steady flight, lift is equal to weight and thrust is equal to drag, so

$$T = drag = \frac{lift}{r} = \frac{weight}{r} = \frac{mass \times g}{r} \ , \tag{A2}$$

where g is the acceleration due to gravity (9.8 m/sec^2) and $mass$ is the total weight of the aircraft (body, battery and payload) in kg. Combining (A1) and (A2) gives

$$E_{fly} = \frac{(m_1+m_2+m_3)\times g}{r} \times d \ , \tag{A3}$$

where m_1 is the mass of the aircraft structure, m_2 is the mass of the aircraft battery and m_3 is the mass of the payload.

An important parameter for battery powered drones is the efficiency for converting battery power to "flight" power delivered by the rotors, denoted η (unitless), where $\eta < 1$. Thus, the energy required from the battery for steady flight is

$$E_{fly} = \frac{(m_1+m_2+m_3)\times g}{\eta r} \times d \ . \tag{A4}$$

Additional energy is consumed by the drone avionics required for safe flight, including communications, sensing, computation, etc. Let P_{avio} be the power required for the aircraft (drone) avionics in joules per second of flight. The energy for avionics (in joules) for a flight of distance d is then

$$E_{avio} = P_{avio} \times \frac{d}{v} \ . \tag{A5}$$

The total energy expended by the aircraft battery (in joules) on a flight of distance d is from equations (A4) and (A5):

$$E_{tot} = \frac{(m_1+m_2+m_3)g}{r\eta} d + P_{avio} \times \frac{d}{v} \ . \tag{A6}$$

The total energy expended per meter of flight Epm is then

$$Epm = \frac{(m_1+m_2+m_3)g}{r\eta} + \frac{P_{avio}}{v} \ . \tag{A7}$$

This is equivalent to the formula presented in D'Andrea (2014) for power

$$\frac{(m_1+m_2+m_3)v}{370\ r\eta} + P_{avio}$$

because power equals $Epm \times v$, and the constant 370 in the denominator of the first term results from substituting in 9.81 for g and measuring speed in km/hr rather than m/sec (3600/9.81 = 367).

Appendix B

The model in Kirschstein (2020) for steady flight is based on the power model in Langelaan et al. (2017) where the power for constant speed flight includes four components for: induced power for lift, power to overcome parasite drag, profile power, and ascending/descending power (based on flight angle θ). This is expressed as a function of the mass and flight angle:

$$P(m_k, v_a, \gamma) = \kappa w T + \frac{1}{2}\rho\left(\sum_{k=1}^{3} C_{D_k} A_k\right) {v_a}^3 + \frac{\rho\sqrt{\varsigma/\pi} n N c c_d}{8} {v_T}^3 \left(1 + 3\left(\frac{v_a}{v_T}\right)^2\right) + (g \sum_{k=1}^{3} m_k) v_a \sin\theta \quad \text{(B1)}$$

where $v_T = \sqrt{\frac{6}{nNcc_l\rho\sqrt{\varsigma/\pi}}}\sqrt{g\sum_{k=1}^{3} m_k}$ is the blade tip speed. The parameter w, like the induced velocity in Stolaroff et al. (2018), is found by solving the following equation

$$w = \frac{T}{2n\rho\varsigma\sqrt{(v_a cos\alpha)^2 + (v_a sin\alpha + w)^2}}, \quad \text{(B2)}$$

where T is from equation (20) and α is from equation (15).

The energy per meter for steady level flight ($\theta = 0$) for a total drone mass of m (including battery and payload if any) with avionics power P_{avio} is

$$Epm = \frac{P(m, v_a, 0)}{\eta v_a} + \frac{P_{avio}}{\eta_c v_a}. \quad \text{(B3)}$$

Kirschstein (2020) uses a total energy efficiency η for drone flight power that includes the motor, transmission and battery charging efficiency, but only the charging efficiency η_c for the avionics.

For a delivery by a drone moving at speed v_a with no wind to a distance d from the depot, the total energy including take-off and ascent at 45° to an altitude of alt, level flight, hovering for time t_{hover}, and then landing, is

$$Epm = \frac{1}{v_a}\left[\frac{P(m,v_a,0)}{\eta} + \frac{P_{avio}}{\eta_c}\right] + \frac{1}{v_a}\frac{alt}{d}\frac{1}{\eta}[P(m,v_a,45°) + P(m,v_a,-45°) - 2P(m,v_a,0)]$$

$$+ \frac{t_{hover}}{d}\left[\frac{P(m,0,0)}{\eta} + \frac{P_{avio}}{\eta_c}\right]. \quad \text{(B4)}$$

The return trip would be the same, but without the payload ($m = m_1 + m_2$). The first term in (B4) is for the level flight, which will usually be the majority of the trip (unless the delivery is for a very short distance), the second term is for the ascending and descending, and the last term is for hovering.

Appendix C. Parameter values used in drone energy use models in a common setting.

Table C.1. Parameters values that are independent of drones

Term	Symbol	Value
Air density [kg/m^3]	ρ	1.225
Acceleration of gravity [m/s^2]	g	9.807
Ratio of headwind to airspeed [unitless]	φ	0
Empty return (1=yes; 0=no)	ϕ	1
Specific energy of the battery [J/kg]	s_{batt}	540,000
Battery power transfer efficiency (from battery to propeller) [unitless]	η	0.7
Safety factor to reserve energy in the battery for unusual conditions [unitless]	f	1.2
Maximum depth of discharge of the battery [unitless]	γ	0.5

Table C.2. Parameters values that depend on drones

Term	Symbol	Small Drone	Large Drone
Number of blades in one rotor [unitless]	N	4	3
Blade chord length [m]	c	0.0157	0.1
Blade lift coefficient [unitless]	c_l	0.271	0.4
Blade drag coefficient (depends on the airfoil)	c_d	0.012	0.075
Number of rotors [unitless]	n	4	8
Spinning area of one rotor [m^2]	ς	0.05067	0.027
Mass of drone body [kg]	m_1	1.07	7
Mass of battery [kg]	m_2	1	10
Mass of payload [kg]	m_3	0.5	7
Projected area of drone body [m^2]	A_1	0.0599	0.224
Projected area of battery [m^2]	A_2	0.0037	0.015
Projected area of payload [m^2]	A_3	0.0135	0.0929
Drag coefficient of drone body [unitless]	C_{D_1}	1.49	1.49
Drag coefficient of battery [unitless]	C_{D_2}	1	1
Drag coefficient of payload [unitless]	C_{D_3}	2.2	2.2
Lift-to-drag ratio [unitless]	r	3	3
Power required for avionics [Watt=J/s]	P_{avio}	0	0
Factor for induced power [unitless]	κ	1	1
Factor for profile power (m/kg)$^{1/2}$	κ_2	0.790	0.683
Factor for profile power associated with speed (m/kg)$^{-1/2}$	κ_3	0.0042	0.0868
Factor for parasite power with payload (kg/m)	κ_4	0.075	0.339
Factor for parasite power without payload (kg/m)	κ_4	0.057	0.214
Base case airspeed [m/s]	v_a	10	10